



**Universiteit  
Leiden**  
The Netherlands

**Multisize electrodes for substrate identification in ischemic cardiomyopathy validation by integration of whole heart histology**

Glashan, C.A.; Tofig, B.J.; Tao, Q.; Blom, S.A.; Jongbloed, M.R.M.; Nielsen, J.C.; ... ; Zeppenfeld, K.

**Citation**

Glashan, C. A., Tofig, B. J., Tao, Q., Blom, S. A., Jongbloed, M. R. M., Nielsen, J. C., ... Zeppenfeld, K. (2019). Multisize electrodes for substrate identification in ischemic cardiomyopathy validation by integration of whole heart histology. *Jacc: Clinical Electrophysiology*, 5(10), 1130-1140. doi:10.1016/j.jacep.2019.06.004

Version: Publisher's Version  
License: [Creative Commons CC BY 4.0 license](https://creativecommons.org/licenses/by/4.0/)  
Downloaded from: <https://hdl.handle.net/1887/4094435>

**Note:** To cite this publication please use the final published version (if applicable).



# Multisize Electrodes for Substrate Identification in Ischemic Cardiomyopathy

## Validation by Integration of Whole Heart Histology

Claire A. Glashan, MD,<sup>a,\*</sup> Bawer J. Tofig, MD,<sup>b,\*</sup> Qian Tao, PhD,<sup>c</sup> Sira A. Blom, BSc,<sup>a</sup> Monique R.M. Jongbloed, MD, PhD,<sup>a,d</sup> Jens C. Nielsen, MD, PhD,<sup>b</sup> Peter Lukac, MD, PhD,<sup>b</sup> Steen B. Kristiansen, MD, PhD,<sup>b</sup> Katja Zeppenfeld, MD, PhD<sup>a</sup>

### ABSTRACT

**OBJECTIVES** This study sought to evaluate the value of combined electrogram (EGM) information provided by simultaneous mapping using micro- and conventional electrodes in the identification of post-myocardial infarction ventricular tachycardia substrate.

**BACKGROUND** Ventricular tachycardias after myocardial infarction are related to scars with complex geometry. Scar delineation and ventricular tachycardia substrate identification relies on bipolar voltages (BV) and EGM characteristics. Early reperfusion therapy results in small, nontransmural scars, the details of which may not be delineated using 3.5 mm tip catheters.

**METHODS** Nine swine with early reperfusion myocardial infarction were mapped using Biosense Webster's QDOT Micro catheter, incorporating 3 microelectrodes at the tip of the standard 3.5 mm electrode. Analysis of EGM during sinus rhythm, right ventricular pacing, and short-coupled right ventricular extrastimuli was performed. The swine were sacrificed and mapping data were projected onto the heart. Transmural biopsies (n = 196) corresponding to mapping points were obtained, allowing a head-to-head comparison of EGM recorded by micro- and conventional electrodes with histology.

**RESULTS** To identify scar areas using standard electrodes, unique cutoff values of unipolar voltage <5.44 mV, BV <1.27 mV (conventional), and BV <2.84 mV (microelectrode) were identified. Combining the information provided by unipolar voltage and BV mapping, the sensitivity of scar identification was increased to 93%. Micro-EGM were better able to distinguish small near-fields corresponding to a layer of viable subendocardium than conventional EGM were.

**CONCLUSIONS** The combined information provided by multisize electrode mapping increases the sensitivity with which areas of scar are identified. EGM from microelectrodes, with narrower spacing, allow identification of near-fields arising from thin subendocardial layer and layers activated with short delay obscured in EGM from conventional mapping catheter. (J Am Coll Cardiol EP 2019;5:1130–40) © 2019 by the American College of Cardiology Foundation.

From the <sup>a</sup>Department of Cardiology, Leiden University Medical Center, Leiden, the Netherlands; <sup>b</sup>Department of Cardiology, Aarhus University Hospital, Aarhus, Denmark; <sup>c</sup>Department of Radiology, Division of Image Processing, Leiden University Medical Center, Leiden, the Netherlands; and the <sup>d</sup>Department of Anatomy and Embryology, Leiden University Medical Centre, Leiden, the Netherlands. \*Drs. Glashan and Tofig contributed equally to this work and are joint first authors. This study was partially supported by an investigator-initiated grant from Biosense Webster (a Johnson and Johnson company). Dr. Tofig has received research support from the Arvid Nilssons Foundation. Dr. Nielsen has received research support from the Novo Nordisk Foundation (grant NNF16OC0018658); and has received an institutional grant from Abbott Denmark. Dr. Lukac has received an institutional grant from Abbott Denmark and Biosense Webster. All other authors have reported that they have no relationships relevant to the contents of this paper to disclose.

The authors attest they are in compliance with human studies committees and animal welfare regulations of the authors' institutions and Food and Drug Administration guidelines, including patient consent where appropriate. For more information, visit the *JACC: Clinical Electrophysiology* [author instructions page](#).

Manuscript received January 7, 2019; revised manuscript received May 10, 2019, accepted June 6, 2019.

Scars after myocardial infarction have complex geometries with variable transmuralities. The thickness of the subendocardial and subepicardial layers of surviving myocardium can also be highly variable, depending on the time to reperfusion and pre-existing collateral arteries (1-7). It has recently been proposed that ventricular tachycardia (VT) circuits are established in areas with a surviving endocardial layer of <2.2 mm and can depend on isthmuses as small as 250  $\mu\text{m}$  (1,8).

SEE PAGE 1141

Substrate-based ablation approaches for scar-related VT rely on 2 pillars: 1) delineation of low-voltage areas by electroanatomical mapping (EAM); and 2) identification of electrograms (EGM) consistent with slow conduction or poor electrical coupling. Electroanatomical bipolar voltage mapping using conventional electrodes ( $BV_C$ ) is considered the invasive reference method for the detection of scar. Currently, a uniformly applied cutoff value of  $BV_C < 1.5$  mV is used (9-12). This cutoff value, however, has only been shown to be effective in identifying compact transmural scars (9,10,13,14). For the detection of small and heterogeneous subendocardial viable layers, mapping with large electrodes and wide interelectrode spacing may be inaccurate due to far-field contamination of local electrical activity by viable myocardium (VM) in subepicardial layers or lateral border zones. It has been theorized that the use of  $BV_C$  (with a more limited field-of-view) rather than unipolar voltage using conventional electrodes ( $UV_C$ ) mapping minimizes the contamination by far-field signal (11,12,15). It has, however, recently been shown that both  $BV_C$  and  $UV_C$  amplitudes are affected by histological changes occurring at distances of more than 4 mm from the endocardial surface (16). The use of bipolar EGM recorded from smaller (or micro) electrodes ( $BV_\mu$ ) may further limit the field-of-view, which may be advantageous in the identification of subendocardial surviving VM (17,18).

Changing the activation wave front and challenging the conduction of surviving tissue through right ventricular (RV) pacing can unmask areas with direction- or rate-dependent conduction delay or block (19). These signals, which are potentially both small and present with only short conduction delay, may be more readily detected using  $BV_\mu$ .

The aim of this study was 2-fold: 1) assess the value of (combined) information provided by  $UV_C$ ,  $BV_C$ , and  $BV_\mu$  mapping in the identification of fibrosis; and 2) determine whether EGM collected with a micro-electrode can be used to identify small areas with (short) conduction delay.

## METHODS

**ANIMAL MODELS.** The study was approved by the Danish Animal Experiments Inspectorate (2017-15-0201-01259) and complied with local institutional guidelines. In 9 domestic Danish swine ( $67 \pm 2$  kg), a myocardial infarction was induced by inflating an intravascular balloon placed after the second diagonal branch of the left anterior descending coronary artery for 65 min before deflation of the balloon. After 10 to 13 weeks, the animals were brought back to the lab for the electrophysiological procedure. (See the [Online Methods](#)).

**EAM AND ABLATION.** Quadripolar catheters were positioned in the right atrial appendage and RV apex for pacing. The ventricular refractory period was determined using RV apex pacing at 500-ms basic train. Endocardial voltage mapping of the left ventricle was performed during stable atrial rate using the QDOT Micro catheter (Biosense Webster, Diamond Bar, California) and the CARTO 3 system version 6.0 (Biosense Webster). For detailed mapping, the fill threshold was set at  $\leq 5$  mm in  $BV_C < 1.5$  mV areas, and  $\leq 15$  mm in  $BV_C > 1.5$  mV areas, as determined by BV mapping using the standard electrode ([Figure 1A](#)). The QDOT Micro catheter integrates 3 microelectrodes at the distal tip of the standard 3.5 mm tip electrode. Each micro-electrode has a surface area of 0.167 mm<sup>2</sup> and is separated from the other 2 electrodes by a distance of 1.755 mm and at 60° such that the 3  $BV_\mu$  collected (between microelectrodes 1-2, 2-3, and 3-1, angle of 60° between the 3 bipoles) are perpendicular to the vector of the  $BV_C$  generated between M1 and M2 (17). Care was taken to only obtain points when the catheter was in stable position (with stable amplitudes on both the conventional and micro-BV EGM), not directly perpendicular to the tissue, and with a contact force  $> 9\text{g}$ . The 3-dimensional coordinates of each point were obtained during diastole.  $UV_C$  EGM were taken against Wilson's Central Terminal and were filtered at a high-pass filter setting of 2 Hz and a low-pass setting of 240 Hz.  $BV_C$  and  $BV_\mu$  EGM were filtered at a high-pass setting of 16 Hz and low-pass setting of 500 Hz. To minimize the effect of wave front propagation direction, the largest of the 3  $BV_\mu$  EGM amplitudes at each recording site was included for analysis.

With the QDOT Micro catheter in a stable position within the scar area ( $BV_C < 1.5$  mV) EGM were

## ABBREVIATIONS AND ACRONYMS

**AUC** = AUC

**$BV_\mu$**  = bipolar voltage using microelectrodes

**$BV_C$**  = bipolar voltage using conventional electrodes

**C1** = first component of electrogram signal (far-field component)

**C2** = second component of electrogram signal (near-field component)

**CI** = confidence interval

**EAM** = electroanatomical mapping

**ECG** = electrocardiogram

**EGM** = electrogram

**IQR** = interquartile range

**RV** = right ventricle

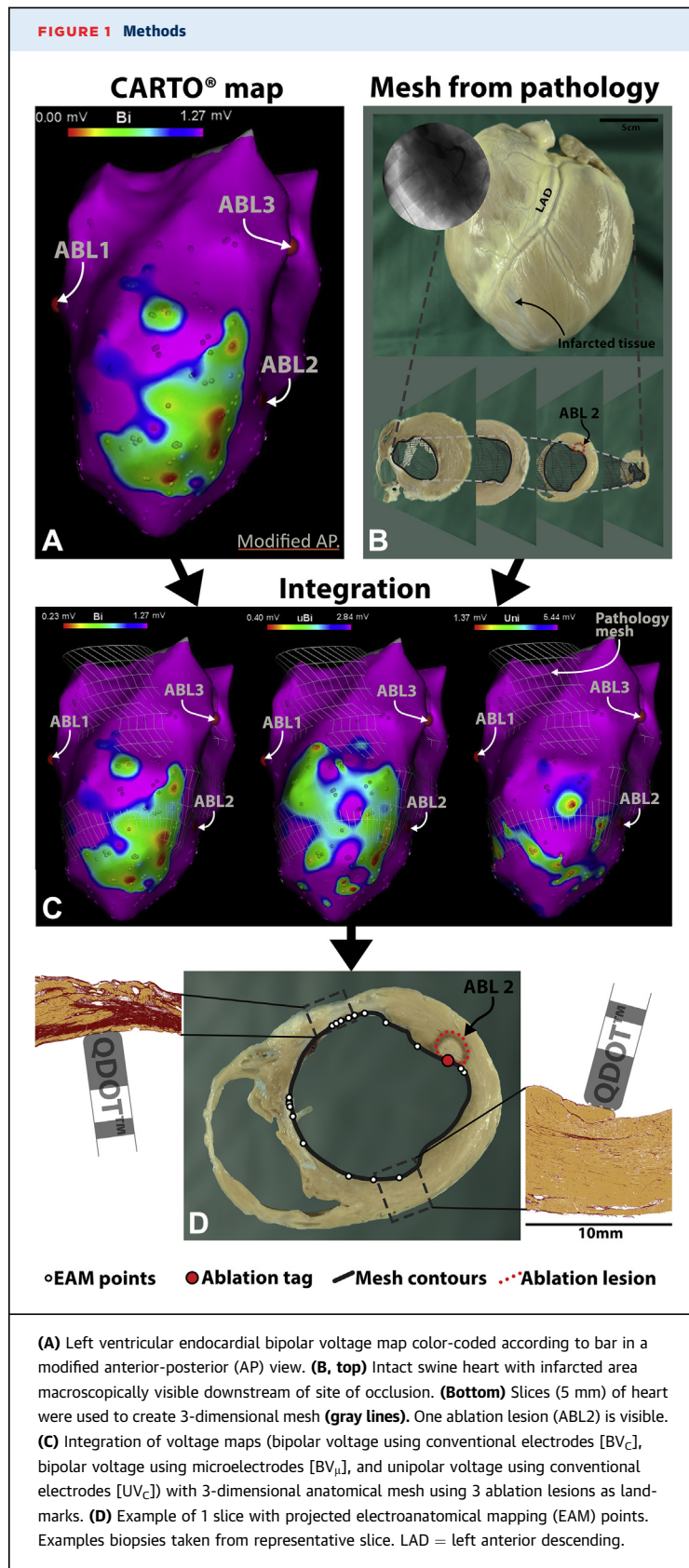
**RVE** = right ventricular extrastimulus

**TB** = transmural biopsies

**$UV_C$**  = unipolar voltage using conventional electrodes

**VM** = viable myocardium

**VT** = ventricular tachycardia



analyzed during atrial pacing (75 beats/min), and then RV pacing at a fixed rate of 500 ms for a train of 5 beats (S1) followed by the application of a single RV extrastimulus (RVE) with a coupling interval of 50 ms above the ventricular refractory period (S2) (19).

EGM were analyzed for the presence of 2 distinct components at baseline, during the basic drive (S1) and after RVE (S2). A lower-frequency potential consistent with far-field was labeled C1, a higher-frequency, single or multiple component consistent with near-field was named C2 (20). A single-component signal, without a clearly distinguishable lower and higher frequency component with conduction delay of more than 10 ms or block in response to RVE (S2) was also categorized as C2.

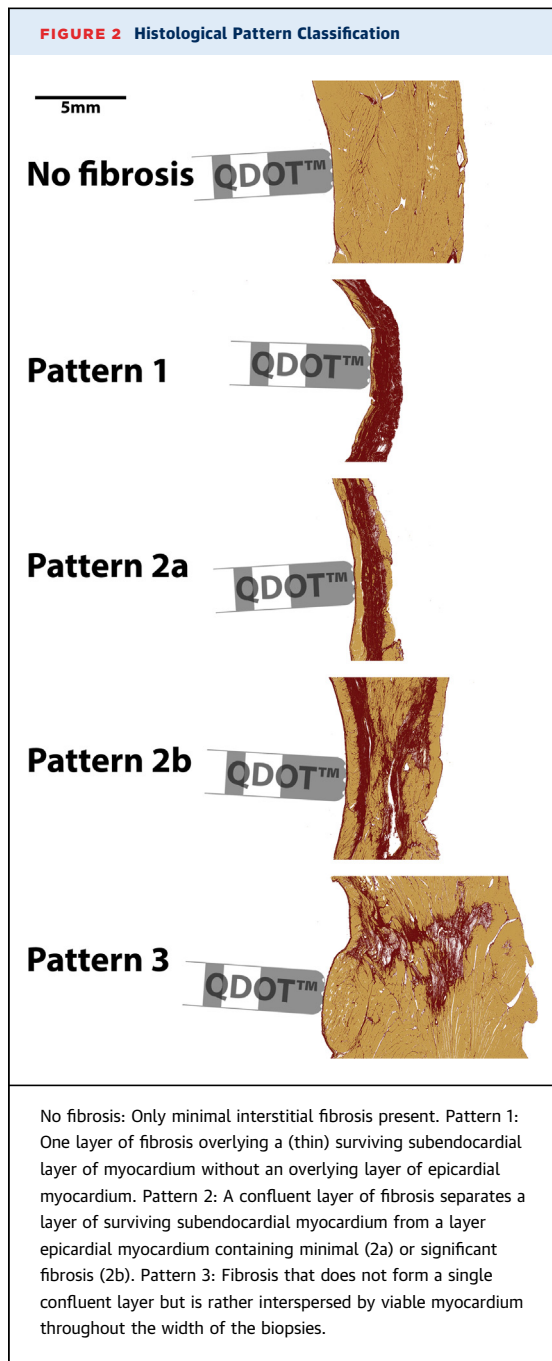
After mapping was performed, 3 ablation lesions, remote from the scar areas were applied using ThermoCool SmartTouch Surround Flow catheter (Biosense Webster) and tagged to allow for accurate integration of mapping data with full heart histology (12).

Euthanasia was performed during general anesthesia with potassium chloride to arrest the heart at end-diastolic phase, which facilitates accurate ex vivo registration with the EAM. The heart was excised, rinsed, and filled with HistOmer (HistOtech, Aarhus, Denmark) (21) to maintain end-diastole dimensions and counteract shrinkage and was fixated in 4% formaldehyde (Sigma-Aldrich, Copenhagen, Denmark) (Figure 1B).

**EX VIVO IMAGE INTEGRATION.** Three-dimensional meshes were created from 5-mm-thick slices of the fixed heart, imported into CARTO, and merged with EAM data (Figures 1A to 1D) (16). (See the Online Methods.)

**HISTOLOGICAL ANALYSIS.** Transmural biopsies (TB) with a width of 10 mm were taken from sites corresponding to nonablation EAM sites (such that each TB corresponded to 1 conventional and 1 microelectrode EGM) and stained with picrosirius to visualize histology with collagen staining red and myocardium yellow (see the Online Methods). Biopsies were visually inspected and classified as having normal (minimal interstitial) or pathological fibrosis (scar). Biopsies with scar were further classified according 3 patterns (see Figure 2 for definitions). Custom software calculated the proportion of fibrosis and the amount of VM (mm<sup>2</sup>) in each transmural biopsy (16).

**STATISTICAL ANALYSIS.** Normally distributed data was reported as mean  $\pm$  SD and not normally distributed data as median and interquartile range (IQR). Categorical data was expressed as proportions or frequencies. Continuous variables were compared



using unpaired Student's *t*-test (parametric) or Mann-Whitney *U*-test (nonparametric) or by using regression analysis. Receiver-operating characteristic curve analysis was performed to determine the optimal cutoff values for assessing a pre-specified amount of VM, defined as the value maximizing the sum of sensitivity and specificity. In the case of single tests, *p* values of <0.05 were considered significant; Bonferroni correction was applied in the case of multiple

testing. Statistical analysis was performed using IBM SPSS version 23, (Armonk, New York).

## RESULTS

**ANIMAL MODELS.** Nine swine were included. Coronary occlusion was performed a median of 85 (IQR: 74 to 98) days before mapping. A median of 220 (IQR: 216 to 260) sinus rhythm points were collected per left ventricle. In 6 swine, programmed RVE was performed. At a total of 88 sites (median of 6 [IQR: 5 to 20] sites per pig), EGM were systematically collected during atrial pacing, RV pacing, and RVE. Image integration was performed successfully in all swine (Figures 1C and 1D) with a high overall registration accuracy of  $5.4 \pm 3.7$  mm.

**HISTOLOGICAL ANALYSIS.** A total of 196 TB were taken (21 [IQR: 20 to 25] per heart) with a mean surface registration error of  $3.1 \pm 1.7$  mm. Of these, 82 had no pathological fibrosis (Figure 1D). These biopsies had a median wall thickness of 8.2 mm (IQR: 6.7 to 10.0), 8.2% (IQR: 7.0 to 9.4) fibrosis, and 69.6 mm<sup>2</sup> (IQR: 59.1 to 84.2) VM. The lower fifth percentile of VM within this group was 47 mm<sup>2</sup>. Of the 114 biopsies with fibrosis, 13 showed pattern 1, 42 pattern 2a, 26 pattern 2b, and 33 pattern 3 (Figure 2).

**VOLTAGES AND CORRESPONDING HISTOLOGY.** During atrial pacing, biopsies with normal amounts of VM ( $\geq 47$  mm<sup>2</sup>) generated UV<sub>C</sub> amplitudes with a median of 7.01 mV (IQR: 5.57 to 8.95; lower fifth percentile: 3.68 mV). The median BV<sub>C</sub> was 2.13 mV (IQR: 1.37 to 3.09; lower fifth percentile: 0.70 mV). The median of the maximum BV<sub>μ</sub> measured was 5.07 mV (IQR: 3.39 to 7.55; lower fifth percentile: 1.82 mV). The BV<sub>μ</sub> measured was significantly higher than the BV<sub>C</sub> measured at each location (*p* < 0.001) with a mean difference of 3.51 mV (95% confidence interval [CI]: 2.96 to 4.06).

During atrial pacing, biopsies with scar and abnormally low amounts of VM generated UV<sub>C</sub>, BV<sub>C</sub>, and BV<sub>μ</sub> of 3.72 mV (IQR: 2.30 to 5.35; lower fifth percentile: 1.24 mV), 0.86 mV (IQR: 0.44 to 1.44; lower fifth percentile: 0.20 mV), and 1.82 mV (IQR: 0.82 to 4.42; lower fifth percentile: 0.38 mV), respectively. Again, the BV<sub>C</sub> was significantly lower than the BV<sub>μ</sub> measured at each location (*p* < 0.001) with a mean difference of 1.60 mV (95% CI: 1.06 to 2.15) (Table 1).

**VOLTAGE AND AMOUNT OF VIABLE MYOCARDIUM.** In all biopsies, there was a positive relationship between the voltages generated under atrial pacing and the amount of VM in the TB. A pairwise analysis showed that for all voltages, there was a difference (*p* < 0.001)

**TABLE 1** Histological and Electroanatomical Characteristics of Biopsies With Normal and Abnormal Amounts of VM

	Normal Amount of VM ( $\geq 47$ mm <sup>2</sup> ) (n = 125)							Abnormal Amount of VM (<47 mm <sup>2</sup> ) (n = 71)						
	Min	Max	Percentile					Min	Max	Percentile				
			5	25	50	75	95			5	25	50	75	95
WT, mm	5.0	14.7	6.2	7.2	8.6	10.0	12.0	1.6	7.7	1.75	2.7	4.1	5.6	7.1
Fibrosis, %	4.5	33.3	5.6	7.5	9.4	14.3	25.9	8.4	87.6	13.1	33.6	43.8	59.8	84.3
VM, mm <sup>2</sup>	47.5	122.9	51.8	59.5	68.1	80.9	101.7	2.1	47.0	3.2	9.1	22.9	35.3	46.2
UV <sub>C</sub> , mV	2.36	11.53	3.68	5.57	7.01	8.95	10.74	0.81	11.21	1.24	2.30	3.72	5.35	7.84
BV <sub>C</sub> , mV	0.50	8.21	0.70	1.37	2.13	3.09	4.31	0.13	4.99	0.20	0.44	0.86	1.44	3.63
BV <sub>μ</sub> , mV	0.76	18.32	1.82	3.39	5.07	7.55	13.29	0.22	12.25	0.38	0.82	1.82	4.42	8.07

BV<sub>μ</sub> = bipolar voltage using microelectrodes; BV<sub>C</sub> = bipolar voltage using conventional electrodes; UV<sub>C</sub> = unipolar voltage using conventional electrodes; VM = viable myocardium; WT = wall thickness.

between the voltages generated by biopsies with 0 to 30 mm<sup>2</sup> VM and those with 30 to 60 mm<sup>2</sup> VM. However, when the 30 to 60 mm<sup>2</sup> group was compared with the 60 to 90 mm<sup>2</sup> group, there was only a significant difference in the BV<sub>C</sub> ( $p = 0.001$ ) and BV<sub>μ</sub> ( $p = 0.008$ ), but not for the UV<sub>C</sub> ( $p = 0.024$ , insignificant after Bonferroni correction for multiple testing). There was no difference between the 60 to 90 mm<sup>2</sup> and 90 to 120 mm<sup>2</sup> groups in any of the voltages. An analysis of all biopsies revealed an associative exponential relationship, supporting this plateauing effect ( $p < 0.001$  for UV<sub>C</sub>, BV<sub>C</sub>, and BV<sub>μ</sub>) (Figure 3, Online Appendix).

Using receiver-operating characteristic analysis, a UV<sub>C</sub> cutoff of 5.44 mV was able to distinguish normal and abnormal amounts of VM with a sensitivity of 77.5% and specificity of 78.4% (area under the curve [AUC] = 0.835). A BV<sub>C</sub> cutoff of 1.27 mV (sensitivity: 71.8%, specificity: 84%, AUC = 0.814) and a BV<sub>μ</sub> cutoff

of 2.84 mV (sensitivity: 66.2%, specificity: 86.4%, AUC = 0.802) were found.

If either low UV<sub>C</sub> or low BV<sub>C</sub> (or both) were considered pathological, the sensitivity could be increased to 87.3% (specificity: 69.6%). If the BV<sub>μ</sub> cutoff was also included such that any location presenting with UV<sub>C</sub> of <5.44 mV, BV<sub>C</sub> of <1.27 mV, or BV<sub>μ</sub> of <2.84 mV was considered pathological, the sensitivity for detecting areas with <47 mm<sup>2</sup> was increased to 93.0% (specificity: 65.6%).

#### RV ELECTRICAL STIMULATION AND EGM ANALYSIS.

A total of 32 TB were taken that corresponded to sites at which RVE was performed. The median voltages measured at these sites during atrial pacing were 0.88 mV (IQR: 0.58 to 1.80) for BV<sub>C</sub> and 2.33 mV (IQR: 1.34 to 4.30) for BV<sub>μ</sub>. The BV<sub>C</sub> recorded during RV pacing was significantly higher than those recorded during atrial pacing with a median of

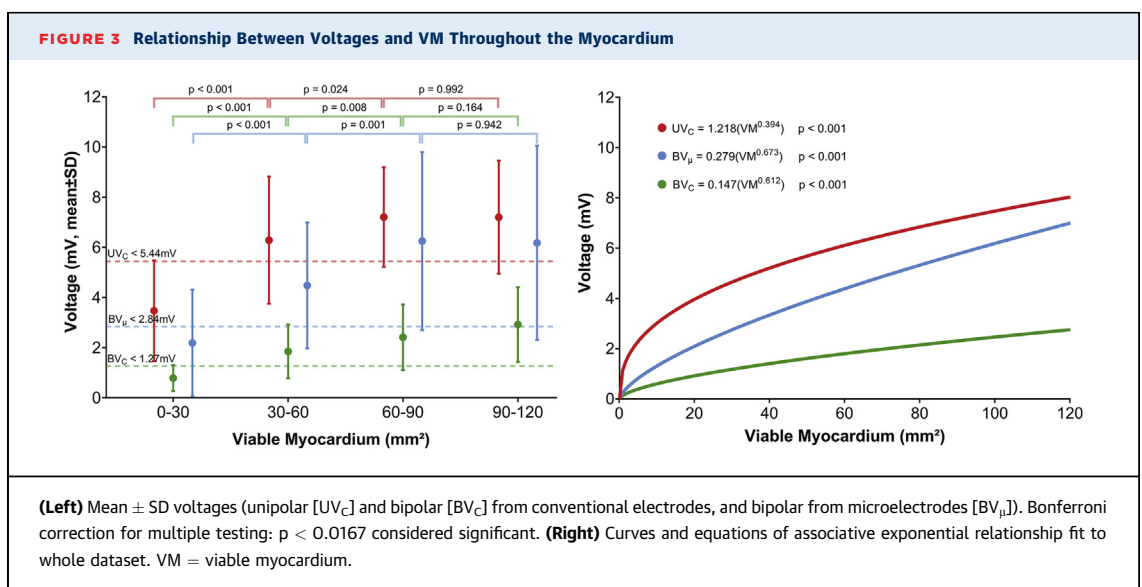
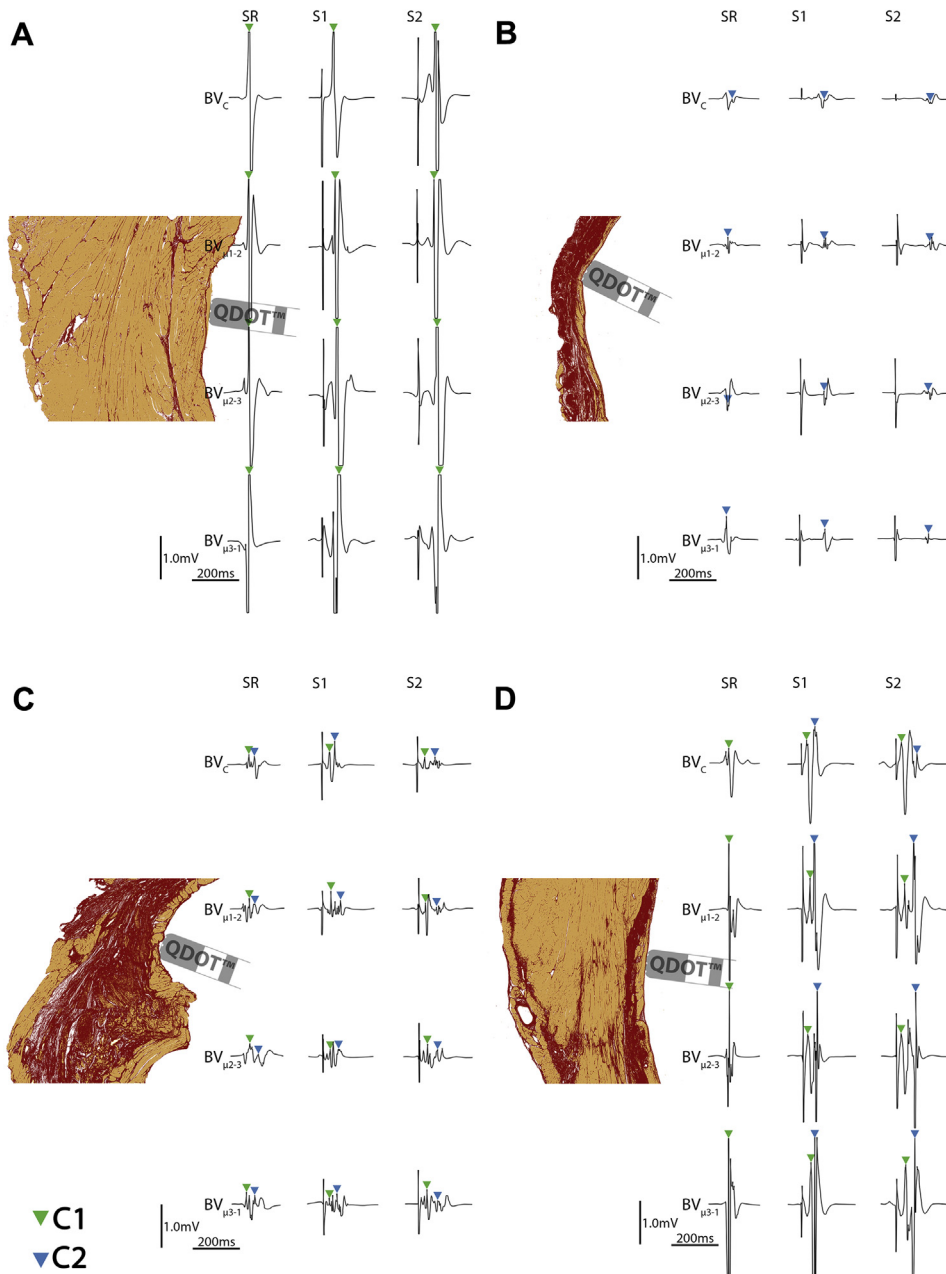


**FIGURE 4** Conventional and Microelectrogram Response to RV Pacing and Extrastimuli: Part 1



All signals visualized on the same scale, signal clipped at 1.7 mV. **(A)** Only the first (far-field) component (C1) is visible (on both conventional and microelectrograms, during both atrial and right ventricular [RV] pacing) (no fibrosis). **(B)** Only the second (near-field) component (C2) is visible (during both atrial and RV pacing) (pattern 1). **(C)** C1 and C2 is visible on all electrograms during both atrial and right ventricular pacing (pattern 2a). **(D)** C1 and C2 visible on all electrodes during RV pacing (pattern 2b). SR = sinus rhythm; other abbreviations as in [Figure 3](#).

1.50 mV (IQR: 1.00 to 2.86; mean difference from atrial pacing: 0.61 mV; 95% CI: 0.16 to 1.06,  $p = 0.009$ ). Interestingly, there was no difference in the amplitude of the  $BV_{\mu}$  measured during RV pacing

compared with during atrial pacing. Median  $BV_{\mu}$  during RV pacing was 3.01 mV (IQR: 1.42 to 5.95; mean difference: 0.36; 95% CI: -0.55 to 1.28;  $p = 0.429$ ).

The QDOT Micro catheter generated 3 microelectrode EGM, the largest of which was taken for all previous analyses. When switching from atrial pacing to RV pacing, the electrode pair that generated the largest amplitude signal changed (mean change of 0.98 mV) at one-half of the sites ( $n = 16$ ).

At locations with only 1 layer of viable myocardium ( $n = 7$ ) (no fibrosis and pattern 1), only 1 component was observed (be it C1 or C2), irrespective of activation (atrial or RV pacing) and electrodes ( $BV_C$  or  $BV_\mu$ ) from which it was collected. Locations without fibrosis generated only 1 large C1 (Figure 4A). Locations with pattern 1 (thin layer of surviving endocardium overlaid with transmural fibrosis) generated only a small C2, in the absence of C1 (Figure 4B).

In the biopsies with patterns 2a, 2b, and 3 ( $n = 25$ ), both C1 and C2 were generated at all but 3 locations. If both C1 and C2 were observed, the 2 components were always visible on at least 1 of the microelectrode EGM (usually on all 3). If both C1 and C2 were visible on both the micro- and conventional EGM (13 sites) both components were already visible during atrial or RV pacing (S1) and the delay between C1 and C2 increased on the application of S2 (Figures 4C and 4D).

Interestingly, at 9 sites, a second component was only discernible on the microelectrodes (Figure 5). In some cases, C2 was visible on the microelectrodes during RV pacing (S1) and on application of the extrastimuli (S2), but it was only visible on the conventional EGM on S2. At these locations, C2 was often partially obscured by the decay artifact of C1 (Figures 5A and 5B). Most significantly, at a number of locations, C2 was only visible on the micro-EGM. Figure 5C shows a typical example of when S2 was only visible during baseline and S1 on the microelectrodes and was blocked on the application of S2. Figure 5D shows an example of C2 becoming visible on the micro-EGM only under S2 while remaining obscured by the decay artifact of C1 in the conventional EGM. These locations showed a more complex fibrotic pattern (most frequently pattern 2b) with either very thin layers of surviving endocardium (Figure 5C) or a thin layer of fibrosis separating the endocardial layer from the overlaying surviving epicardial layer (Figure 5D, Online Appendix).

## DISCUSSION

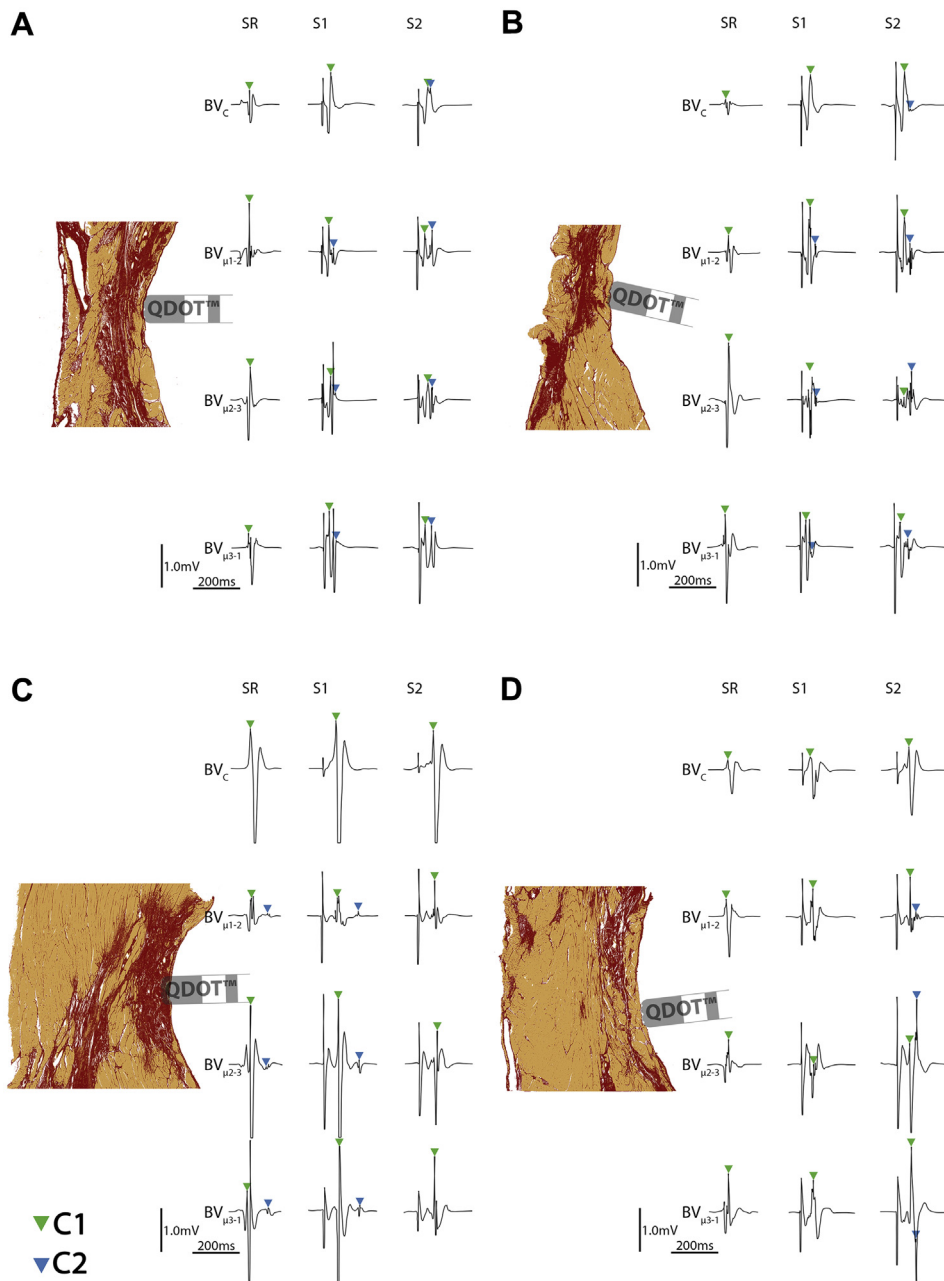
This study is the first to couple voltage mapping data and EGM characteristics simultaneously collected with both conventional and microelectrodes during sinus rhythm, RV pacing, and RVE with the true gold standard for fibrosis identification—histology with high registration accuracy.

**MAIN FINDINGS.** 1) All voltage amplitudes ( $UV_C$ ,  $BV_C$ , and  $BV_\mu$ ) are affected by the amount of viable myocardium present at a given location. 2) By being able to definitively identify areas of fibrosis using histology, we have been able to generate cutoff values for  $UV_C$ ,  $BV_C$ , and  $BV_\mu$  (5.44 mV, 1.27 mV, and 2.84 mV, respectively) for identifying normal amount of viable myocardium. Combining information provided by  $UV_C$ ,  $BV_C$ , and  $BV_\mu$  increases the sensitivity of voltage mapping in identifying areas of abnormally low VM. 3) The spatial relationship of the 3 microelectrode recordings, and the selection of the EGM with the largest amplitude, may allow for partial compensation of wave front propagation dependency. 4) EGM produced by microelectrodes have relatively higher amplitudes allowing for the identification of smaller near-field components. Microelectrode EGM can detect the activation of a subendocardial layer even if the delay is so slight that it occurs within the duration of the far-field EGM (on the conventional EGM).

**VOLTAGE MAPPING USING MULTISIZE ELECTRODE.** In the current study we have shown that BV amplitudes recorded with microelectrodes are significantly larger than the BV amplitudes measured using conventional mapping catheters, irrespective of whether this was in areas with normal versus abnormal amounts of VM. Accordingly, we cannot use the same cutoff value for both conventional and microelectrode BV amplitudes. If a single cutoff value is used (at all), a different value should be defined for each electrode size used. One possible reason for these higher amplitudes is the use of smaller electrodes. UV signals collected from smaller electrodes should overlap less and as such the resultant BV signal should suffer less cancellation. Furthermore, as the QDOT Micro catheter combines 3 microelectrodes, there is a significantly high chance that 1 of these pairs will be in line with the depolarization wave front. Changing the activation wave front (from atrial pacing to RV pacing) led to no significant change in the  $BV_\mu$  amplitude measured in a small group ( $n = 32$ ) while it led to a significant change in the amplitude of the  $BV_C$  measured.

In areas with normal amounts of viable myocardium, we recorded median  $BV_\mu$  of 5.07 mV with a lower fifth percentile of 1.82 mV. This is higher than the  $BV_\mu$  measured in healthy swine by Leshem et al. (17) who found a mean  $BV_\mu$  of  $3.8 \pm 2.3$  mV (and a lower fifth percentile of 1.3 mV). There are several aspects that may contribute to the observed differences. A possible reason may lie in the swine used: Leshem et al. (17) used swine that weighed 56 kg at

**FIGURE 5** Conventional and Microelectrogram Response to RV Pacing and Extrastimuli: Part 2

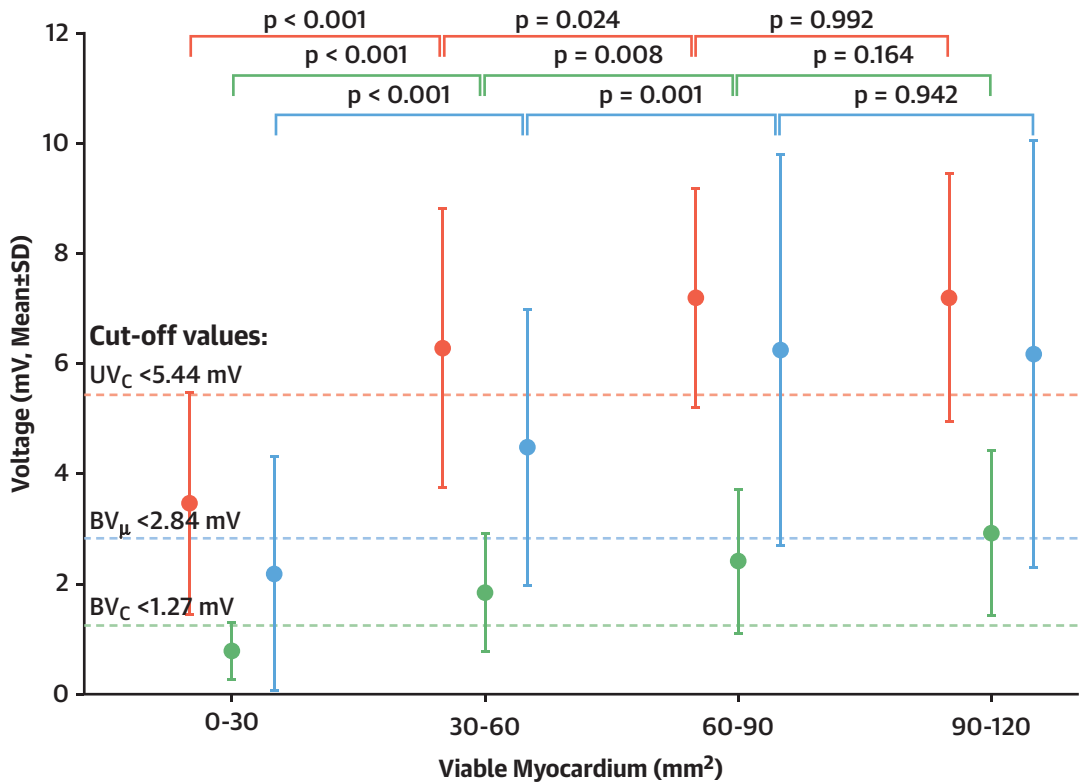


**(A)** C2 is visible on microelectrograms during S1, and C2 is only visible on conventional electrogram during S2 (pattern 2b). **(B)** C2 is only visible on conventional electrogram during S2 and partially obscured in decay artifact of C1 (pattern 2a). **(C)** Small amplitude C2 is only visible in microelectrograms at baseline and during S1 and is blocked on S2 (pattern 2b). **(D)** C2 is only visible on microelectrograms during application of S2 and is not visible in decay artifact of conventional electrogram (pattern 2b). Abbreviations as in [Figures 3 and 4](#).

the time of mapping to generate normal values (E. Leshem, personal communication, April 2019), whereas our swine averaged 86 kg at the time of mapping. Furthermore, in this study, care was taken

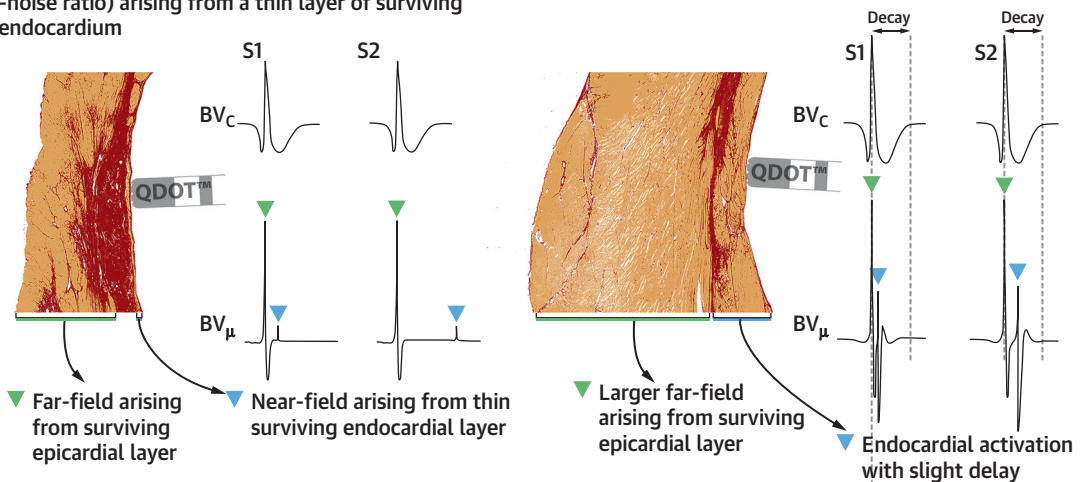
to ensure that all points were acquired with contact force of >9g, which was facilitated by a carotid approach (which may also influence the catheter orientation and angle of incidence, which may affect

**CENTRAL ILLUSTRATION Advantages of Multisize Electrode Mapping in Ischemic Cardiomyopathy**



At a given location relatively higher amplitudes generated by micro-electrodes, compared to conventional electrode, allowing for identification of smaller near-field components (higher signal-to-noise ratio) arising from a thin layer of surviving endocardium

Micro-EGMs are narrower, sharper signals with a small decay artifact (higher temporal resolution) allowing for the identification of a second component hidden in the decay artifact of conventional EGMs



Glashan, C.A. et al. J Am Coll Cardiol EP. 2019;5(10):1130-40.

Relationship between voltages (from conventional electrode tip [unipolar voltage and bipolar voltage ( $BV_c$ )] and from microelectrode [ $BV_\mu$ ]) and viable myocardium generated at a given location. Positive association between  $BV_\mu$  and viable myocardium  $BV_\mu$  is sensitive to changes in viable myocardium occurring further away from the catheter tip. Cutoff values generated through receiver-operating characteristic analysis shown. Schematic shows additional advantage of using microelectrodes.

the voltages recorded). Leshem et al. (17), using an inguinal approach, allowed for variation between 5g and 40g, which may also have contributed to the lower  $BV_{\mu}$  recorded.

All 3 voltages appear to be sensitive to change in VM occurring at any site throughout the myocardial wall. An associative exponential relationship was seen for all 3 voltages ( $UV_C$ ,  $BV_C$ , and  $BV_{\mu}$ ). Interestingly, if the subgroups are compared, this saturation appears to occur later for  $BV_{\mu}$  and  $BV_C$  than for  $UV_C$ . This maintenance of a positive relationship between VM and  $BV_{\mu}$  suggests that  $BV_{\mu}$  is influenced by increases in viable myocardium across the wall, rather than only the subendocardial layer.

By being able to use the true gold standard for scar identification—histology—we have been able to generate more clinically applicable cutoff values. We found that a  $UV_C$  cutoff of 5.44 mV was best able to distinguish areas of reduced VM. A  $BV_C$  of 1.27 mV and a  $BV_{\mu}$  of 2.84 mV were also best able to identify these areas. Interestingly, by considering all voltages, rather than focusing on areas below a single cutoff value, we could increase the sensitivity of voltage mapping to 93% (as opposed to 76%, 69%, and 64% if using the single cutoffs of  $UV_C$  of <5.44 mV,  $BV_C$  of <1.27 mV, or  $BV_{\mu}$  of <2.84 mV, respectively). The information provided by  $UV_C$ ,  $BV_C$ , and  $BV_{\mu}$  is likely slightly different and complimentary and the respective maps may show slightly different low-voltage areas in scars with complex geometry and transmural (Figure 1C).

**IDENTIFY EGM CONSISTENT WITH SLOW CONDUCTION USING MULTISIZE ELECTRODES.** When performing RVE, it became apparent that near-field (C2) components were more readily visualized on the microelectrodes. We hypothesize that the strength and additional benefit of the microelectrodes are in 2 aspects. 1) The signals generated by the microelectrodes are of a relatively higher amplitude, compared with those generated by the conventional electrodes at any given location. This allows for identification of small near-field component arising from thin layer of surviving endocardium (higher signal-to-noise ratio), which are not visualized on conventional EGM (Figure 3, Central Illustration). 2) The EGM produced by the microelectrode are more precise with respect to time (greater temporal resolution), resulting in narrower, sharper signals with a smaller decay artifact that allows for the identification of a second component that is hidden in the decay artifact of conventional electrodes (Figure 5, Central Illustration). These second components may

even be visible during sinus rhythm; eliminating the need for RVE in some cases. The application of RVE can further unmask poorly coupled subendocardial myocardium arising from a thin layer that may be too small to be visible on conventional electrodes. This may be particularly important in the detection of the thin layer of myocardium needed to sustain VT. It has recently been shown that most VT are established in VM with a thickness of  $\leq 2.2$  mm (8), which may be difficult to detect with conventional, large-tip electrodes.

**STUDY LIMITATIONS.** Whereas cutoff values in a swine infarct model were identified in this study, these values need to be validated in humans. The histology of 2-dimensional slices corresponding to the mapping points were taken. However, voltage mapping is influenced by the myocardial tissue surrounding the catheter tip in all 3 dimensions. Furthermore, the exact orientation of the catheter to tissue and wave front propagation is unfortunately not known. In this study, only fibrosis amount and patterns were assessed, other histopathological characteristics may also play a role in arrhythmogenesis and should be explored. Although the relationship between voltage mapping and histology has been elucidated, the specific histological characteristics of VT-related sites have not been explored.

## CONCLUSIONS

Using a post-infarct model, the following cutoff values for the QDOT Micro catheter have been established:  $UV_C$  of <5.44 mV,  $BV_C$  of <1.27 mV,  $BV_{\mu}$  of <2.84 mV. The combined information provided by multisize electrode voltage mapping increases the sensitivity with which areas of scar are identified. The use of microelectrodes allows for the identification of small near-field components that are either not detected by the large-tipped electrodes or are obscured by the decay artifact produced in conventional EGM. The use of the microelectrode catheter not only improves the detection of areas of low VM, but also provides more detailed information about areas of (functional) slow conduction.

**ACKNOWLEDGMENT** The authors thank J.C. Sorensen for graciously allowing us to use HistOmer (21) to embed our tissue.

**ADDRESS FOR CORRESPONDENCE:** Dr. Katja Zepfenfeld, Leiden University Medical Center, Department of Cardiology (C-05-P), P.O. Box 9600, 2300 RC Leiden, the Netherlands. E-mail: [K.Zepfenfeld@lumc.nl](mailto:K.Zepfenfeld@lumc.nl).

## PERSPECTIVES

**COMPETENCY IN MEDICAL KNOWLEDGE 1:** All voltages ( $UV_C$ ,  $BV_C$ , and  $BV_\mu$ ) are influenced by changes in VM occurring across the myocardial wall, not just within the subendocardial layer. Combining the information provided by multisize electrodes may allow for more accurate substrate delineation, particularly in the case of nontransmural or patchy scar.

**COMPETENCY IN MEDICAL KNOWLEDGE 2:** Microelectrode signals are able to identify small near-field components that are not detected by the large-tipped electrodes or are obscured by the decay artifact produced in conventional EGM. Using these

microelectrodes may allow for better identification of (functional) slow conducting areas and thereby improve ablation outcomes. This may be of particular importance in patients with early reperfusion infarctions where the large surviving epicardial layer hampers mapping using conventional electrodes.

**TRANSLATIONAL OUTLOOK:** Further studies in humans are needed to validate the voltage amplitudes generated in this swine model. Furthermore, further studies are needed to explore the relationship between histological characteristics and VT-related sites as identified using microelectrodes.

## REFERENCES

- de Bakker JM, Coronel R, Tasseron S, et al. Ventricular tachycardia in the infarcted, Langendorff-perfused human heart: role of the arrangement of surviving cardiac fibers. *J Am Coll Cardiol* 1990;15:1594-607.
- de Bakker JM, van Capelle FJ, Janse MJ, et al. Slow conduction in the infarcted human heart: 'Zigzag' course of activation. *Circulation* 1993;88:915-26.
- Bolick DR, Hackel DB, Reimer KA, Ideker RE. Quantitative analysis of myocardial infarct structure in patients with ventricular tachycardia. *Circulation* 1986;74:1266-79.
- Dillon SM, Alessie MA, Ursell PC, Wit AL. Influences of anisotropic tissue structure on reentrant circuits in the epicardial border zone of subacute canine infarcts. *Circ Res* 1988;63:182-206.
- Pop M, Ghugre NR, Ramanan V, et al. Quantification of fibrosis in infarcted swine hearts by ex vivo late gadolinium-enhancement and diffusion-weighted MRI methods. *Phys Med Biol* 2013;58:5009-28.
- Beltrami CA, Finato N, Rocco M, et al. Structural basis of end-stage failure in ischemic cardiomyopathy in humans. *Circulation* 1994;89:151-63.
- de Bakker JM, van Capelle FJ, Janse MJ, et al. Reentry as a cause of ventricular tachycardia in patients with chronic ischemic heart disease: electrophysiologic and anatomic correlation. *Circulation* 1988;77:589-606.
- Pashakhanloo F, Herzka DA, Halperin H, McVeigh ER, Trayanova NA. Role of 3-dimensional architecture of scar and surviving tissue in ventricular tachycardia: insights from high-resolution ex vivo porcine models. *Circ Arrhythm Electrophysiol* 2018;11:e006131.
- Wroblewski D, Houghtaling C, Josephson ME, Ruskin JN, Reddy VY. Use of electrogram characteristics during sinus rhythm to delineate the endocardial scar in a porcine model of healed myocardial infarction. *J Cardiovasc Electrophysiol* 2003;14:524-9.
- Reddy VY, Wroblewski D, Houghtaling C, Josephson ME, Ruskin JN. Combined epicardial and endocardial electroanatomic mapping in a porcine model of healed myocardial infarction. *Circulation* 2003;107:3236-42.
- Desjardins B, Yokokawa M, Good E, et al. Characteristics of intramural scar in patients with nonischemic cardiomyopathy and relation to intramural ventricular arrhythmias. *Circ Arrhythm Electrophysiol* 2013;6:891-7.
- Piers SR, Tao Q, van Huls van Taxis CF, Schalij MJ, van der Geest RJ, Zeppenfeld K. Contrast-enhanced MRI-derived scar patterns and associated ventricular tachycardias in nonischemic cardiomyopathy: implications for the ablation strategy. *Circ Arrhythm Electrophysiol* 2013;6:875-83.
- Callans DJ, Ren JF, Michele J, Marchlinski FE, Dillon SM. Electroanatomic left ventricular mapping in the porcine model of healed anterior myocardial infarction: correlation with intracardiac echocardiography and pathological analysis. *Circulation* 1999;100:1744-50.
- Wijnmaalen AP, Schalij MJ, von der Thülen JH, Klautz RJ, Zeppenfeld K. Early reperfusion during acute myocardial infarction affects ventricular tachycardia characteristics and the chronic electroanatomic and histological substrate. *Circulation* 2010;121:1887-95.
- Desjardins B, Morady F, Bogun F. Effect of epicardial fat on electroanatomical mapping and epicardial catheter ablation. *J Am Coll Cardiol* 2010;56:1320-7.
- Glashan CA, Androulakis AFA, Tao Q, et al. Whole human heart histology to validate electroanatomical voltage mapping in patients with non-ischaemic cardiomyopathy and ventricular tachycardia. *Eur Heart J* 2018;39:2867-75.
- Leshem E, Tschabrunn CM, Jang J, et al. High-resolution mapping of ventricular scar: evaluation of a novel integrated multielectrode mapping and ablation catheter. *J Am Coll Cardiol EP* 2017;3:220-31.
- Leshem E. High-resolution mapping of ventricular scar. *J Am Coll Cardiol EP* 2017;3:220-31.
- de Riva M, Naruse Y, Ebert M, et al. Targeting the hidden substrate unmasked by right ventricular extrastimulation improves ventricular tachycardia ablation outcome after myocardial infarction. *J Am Coll Cardiol EP* 2018;4:316-27.
- Jais P, Maury P, Khairy P, et al. Elimination of local abnormal ventricular activities: a new end point for substrate modification in patients with scar-related ventricular tachycardia. *Circulation* 2012;125:2184-96.
- Bjarkam CR, Pedersen M, Sorensen JC. New strategies for embedding, orientation and sectioning of small brain specimens enable direct correlation to MR-images, brain atlases, or use of unbiased stereology. *J Neurosci Methods* 2001;108:153-9.

**KEY WORDS** histology, microelectrodes, myocardial infarction, substrate ablation, swine, ventricular tachycardia

**APPENDIX** For an expanded Methods section as well as a supplemental table and figure, please see the online version of this paper.